INT. COMM. HEAT MASS TRANSFER 0735-1933/86 $3.00 + .00
Vol. 13, pp. 535-543, 1986 ©Pergamon Journals Ltd. Printed in the United States

INTERFACIAL INSTABILITIES OF AIR-DRIVEN LIQUID FILMS

I. Mudawwar
Boiling and Two-Phase Flow Laboratory
School of Mechanical Engineering
Purdue University
West Lafayette, Indiana 47907

(Communicated by J.P. Hartnett and W.J. Minkowycz)

ABSTRACT

Experiments were conducted to develop a better understanding of stress distribution at the interface of air-driven liquid films using solid waves similar in shape to the interfacial disturbances. Pressure and velocity measurements around the contour of each wave indicate that the air flow separates from the downstream side of the wave. These results suggest that the mass and momentum transport of liquid films in parallel two-phase flow may be dominated by form drag forces exerted on the interfacial waves rather than shear forces.

Introduction

Considerable attention has been given by many researchers to the problem of predicting spatial variations of the shear stress and pressure at the interface of a liquid film driven by parallel gas flow. For small wave amplitudes such variations are sinusoidal [1-3]. Thus they can be described by well established linearized momentum equations. However, according to more recent experimental results [4], separation and flow reversal occur over solid wavy walls for wave amplitude to wavelength ratios in excess of 0.0165. Thus, it is quite possible that the motion of a "shear-driven" film is actually dominated by form drag.

The present study focuses on the mechanisms of interfacial instability of an air-driven liquid film, and on the spatial variation of pressure along the air-liquid interface.

Experiments

The test facility, which is shown in Fig.1, consisted of a wind-tunnel, air nozzle, liquid reservoir and feeding section, a flow channel and a measurement cylinder. A 1/4-hp air blower equipped with a speed controller provided a wide range of air speeds into the flow channel. The end of the diffuser was 100 cm by 100 cm in cross section where several screens were mounted in parallel to eliminate vorticity effects created by the air blower. The air nozzle at the inlet to the flow channel was covered with a smooth layer of Mylar to avoid local flow separation. It provided a flow area reduction of 30.48 cm by 30.48 cm to 4.76 cm by 10.16 cm over a distance of 30.48 cm. Nozzle flow calculations suggested that the boundary layer near the nozzle outlet was very thin and could be assumed to start at the inlet to the flow channel. Rubber damping plates were installed at both ends of the nozzle to minimize vibration induced by the air blower.

The rectangular flow channel consisted of an inlet liquid feeder and as many as three identical downstream sections 68.68 cm long and 5.08 by 10.16 cm in cross section. The side walls and upper cover of each of these sections were fabricated of 12.7 mm thick plexiglass for optical accessibility. Liquid injection into the channel was provided by a rectangular groove machined in the bottom wall of the feeder at a 45 degree angle with respect to the air flow. The groove width was adjustable over a range of 0.318 - 0.794 mm by means of special adapters. The liquid front at the groove was protected against instabilities created by air drag by a 0.32 mm steel plate which extended between the groove and the air nozzle. Solutions of various concentrations of glycerin in water were tested in these experiments. Gravity feeding was preferred to using a pump to prevent the generation of flow instabilities by mechanical vibrations. The liquid was stored in a large reservoir mounted on an elevated platform above the flow channel. Liquid injection into the channel was controlled by a valve installed at the bottom of the feeder. The liquid flow was brought to stagnation inside a reservoir attached to the bottom of the feeder to achieve uniform flow at the injection groove. The liquid flow rate was measured by collecting the film inside a calibrated cylinder at the end of the channel. The channel sections were carefully flanged together to ensure a smooth bottom wall. Pressure taps were mounted through the cover of each section. Several pitot-static and stagnation probes

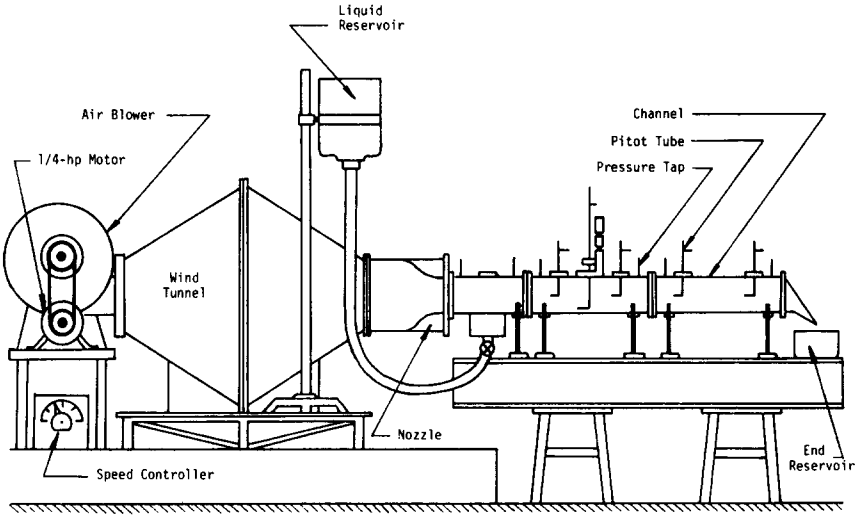

FIG 1 Schematic diagram of the experimental facility

were utilized for velocity measurements. Velocity profiles near the bottom wall were obtained using a 0.50 mm boundary layer tube with a flattened tip to minimize the shift in the effective center of measurement. A vertical micrometer translation stage with a 0.01 mm accuracy was used to control the elevation of the boundary layer probe. The bottom walls of the channel sections were fabricated of aluminum. For some tests, chilled ethylene glycol was circulated inside copper tubing soldered to the bottom side of the aluminum plates to create temperature and viscosity gradients across the film.

A specially instrumented plate was fabricated to facilitate flow and pressure measurements around solid waves constructed of a mixture of clay and epoxy. The shape of each wave was determined from photographs of actual liquid waves. The pressure distribution on the surface of the solid wave was obtained by three strategically located 0.50 mm diameter probes as shown in Fig.2. Several tests were performed to locate the first probe at the point of highest stagnation pressure. A second probe was located at the wave crest followed by a third, which was mounted at the inflection point downstream the crest. Three additional pressure probes were mounted at equal distances of

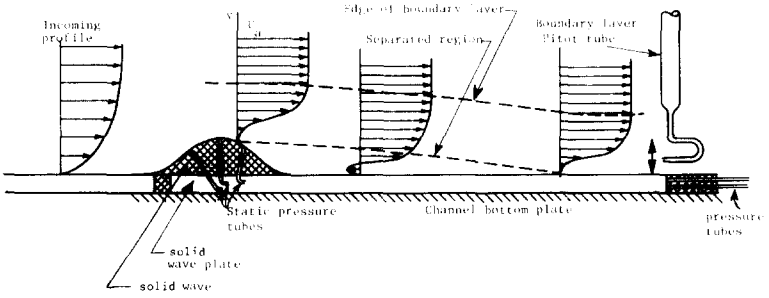

FIG 2 Sectional diagram of the solid wave plate showing locations of the static pressure taps.

5.08 cm behind the wave crest to monitor pressure distribution within the separation region. The entire plate containing the solid waves was connected to the bottom wall of the channel. Velocity profiles were measured at various axial locations relative to the solid waves using boundary layer probes.

Results and Discussion

Experimental Observations

Studies of the film characteristics were made for film mass flow rates of 3×10^{-4} to 1×10^{-2} kg/ms and for air speeds between 8.0 and 30 m/s. Both smooth and wavy film flow was observed over this range of parameters. Changes in the characteristics of the interfacial disturbances were primarily induced by variations of air speed. At very low speeds the film interface was smooth and stable indicating shear-driven film motion. With increased air speed the interface was no longer smooth and, as can be seen in Fig.3, uniform sinsoidal waves were observed. The wave crests spanned the full width of the channel and moved at a fairly constant speed. Increasing the air speed somewhat destroyed the uniformity of the sinusoidal waves, but the distance between adjacent crests remained roughly equal to the width of each wave. Accounting for the distortion of perspective due to the camera optics, Fig.3 shows the wave crests propogating in parallel rows while in Fig.4, which corresponds to a higher air speed, some three-dimensional disturbances can be observed. For higher air speeds, the wave shape was altered, with the wave width becoming significantly smaller than the separation between crests. Representative pho-

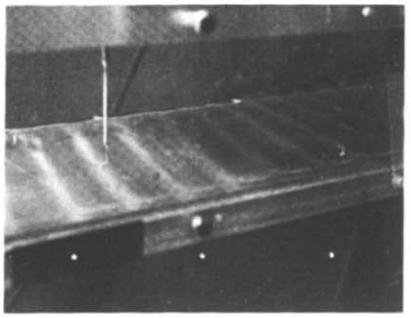

FIG 3 Liquid film in the sinusoidal regime (flow is from left to right).

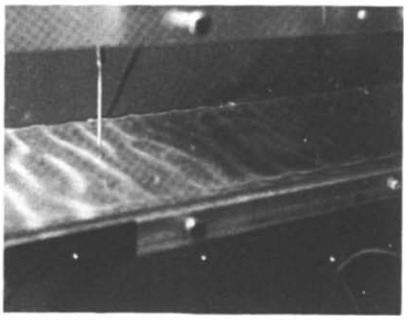

FIG 4 Liquid film flow in the quasi-sinusoidal regime (onset of three dimensional disturbances).

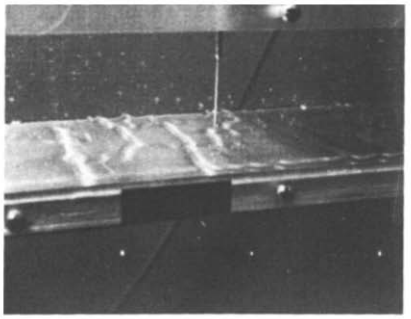

FIG 5 Liquid film flow in the ripple regime (large wavelength).

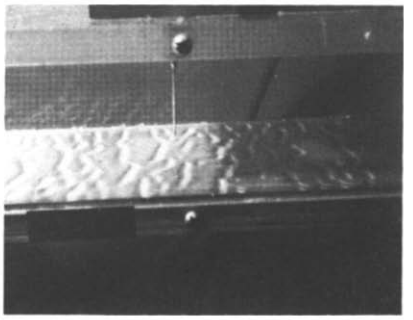

FIG 6 Liquid film flow in the ripple regime (small wavelength).

tographs of this type of disturbance are shown in Figs.5 and 6. In this regime, the wave did not usually span the full channel width. In addition, the waves developed into ripples of sharp curvature and took on an almost solitary character. Advancing ripples seemed to capture slower upstream ripples to form larger and faster ripples. These disturbances dominated the motion of the film over most of the air speed range considered in this study. Thus the ripple flow may represent a "fully-developed" interfacial disturbance regime associated with high air speeds.

To investigate the effect of ripples on mass transport within the film, fine saw dust was mixed with the glycerin solution and traced along the flow

channel. Particles scattered in the substrate film between individual ripples were practically stagnant with respect to the fast moving ripples. Once a particle was captured by an advancing ripple, it was then driven at the ripple speed over a considerable distance before being rejected into the substrate film behind it. Similar effects were observed using the flow measurement cylinder at the end of the channel. The wavy motion seemed to supply discrete masses of liquid upon the arrival of ripples which indicates the dominating role of these ripples in transporting the bulk of the liquid flow.

Solid Wave Results

The sharp curvature associated with the shape of individual liquid ripples indicates that form drag plays a significant role in the motion of the film. Since the ripples move very slowly (<0.10m/s) relative to air (>10m/s), the interface could be assumed to exert a steady disturbance to the airside flow. To provide more quantitative data for surface stresses, pressure and velocity measurements were performed using solid ripples whose curvature resembled that of typical liquid ripples. The shape of the solid wave was characterized by its length L, height h, and the wave profile function

$$y = \frac{h}{2}\left[1 + \sin\frac{2\pi}{L}(x - L/4)\right] \tag{1}$$

Pressure measurements for two solid ripples are shown in Fig.7. The data indicate a pressure distribution similar to that obtained for crossflow over a cylinder with separation occurring at its trailing side. Approximate values of the drag force on the ripple were obtained by using the measured pressure at the wave surface and through the extent of the separation region to define a piece-wise linear pressure function. The drag force on the wave was computed using the following equation:

$$F/w \equiv \int_0^L \left[p - p_a\right] \frac{dy}{dx}\, dx \tag{2}$$

where F/w is the drag force per unit width and $(P-P_a)$ is the measured pressure at the solid wave surface minus the local free-stream pressure measured at the upper channel cover directly above the wave. The drag coefficient was defined

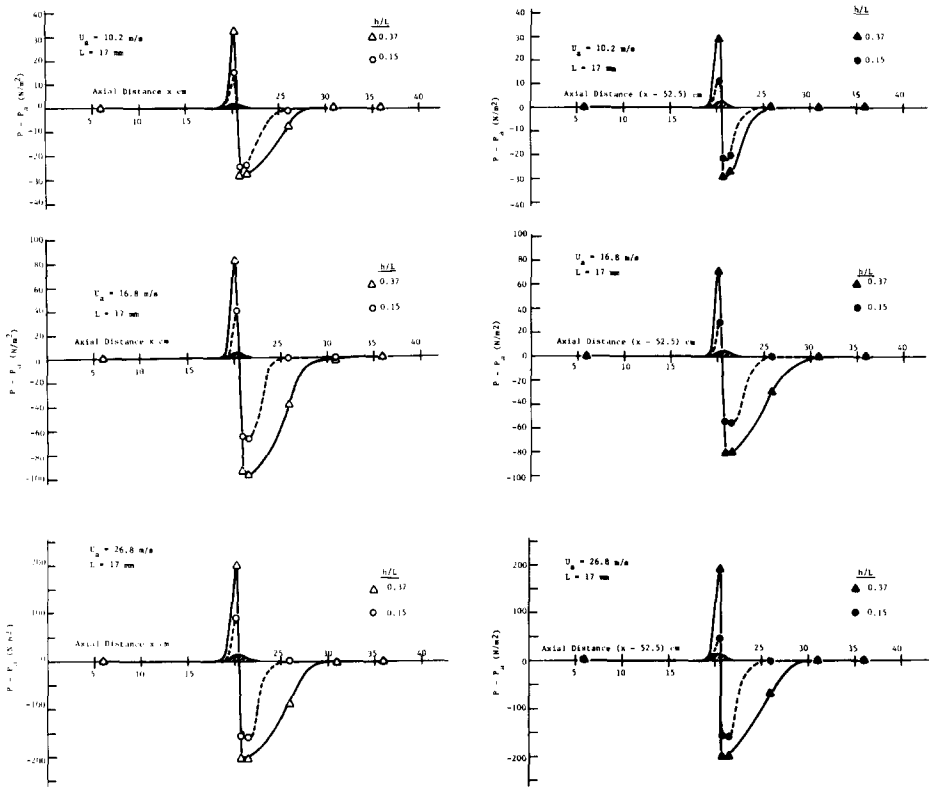

FIG 7 Static pressure distribution around a solid wave for various wave shapes, air speeds and axial positions.

as

$$C_D \equiv \frac{F/w}{h[\frac{1}{2}\rho_a U_a^2]} \tag{3}$$

where ρ_a and U_a represent the density and velocity of the free air stream, respectively. The variation of the drag coefficient with airside Reynolds number for two wave shapes is shown in Fig.8. This figure clearly indicates a significant increase in the form drag with an increase of wave protrusion into the air boundary layer.

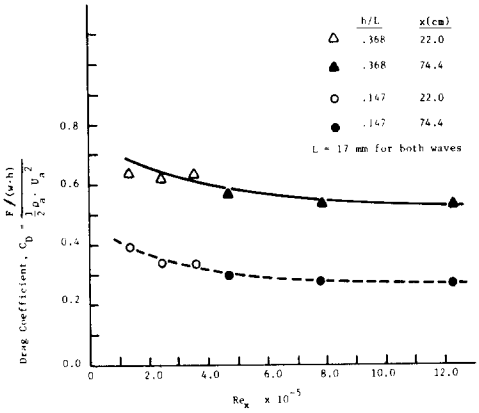

FIG 8 Variation of the drag coefficient for air flow over a solid wave with Reynolds number based on the distance from the channel inlet.

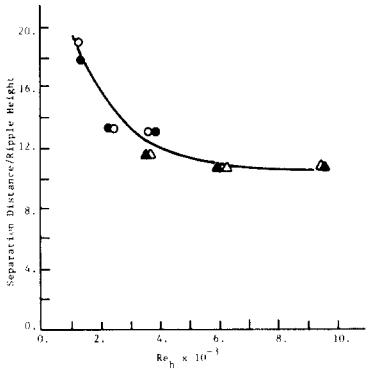

FIG 9 Variation of the ratio of separation distance to wave height with Reynolds number based on wave height. Results for two wave heights and two axial locations are shown (see Fig. 8 for key to symbols).

To determine the separation distance behind the solid wave, the solid wave plate was slightly displaced in the axial direction and fixed in place while the boundary layer probe was translated in a direction normal to the plate. The reattachment point corresponded to the position at which the probe failed to detect changes in the total head in the vicinity of the plate. This method was successful to within 3 mm for separation distances of the order of 50 mm. Variation of the separation distance for two wave shapes are is shown in Fig.9. These results reveal the existence of a wide separation region behind the waves, a fact which explains some observations of the behavior of liquid waves in the ripple flow regime. The results of Figs.8 and 9 indicate that when ripples approach each other to the extent where the trailing ripple falls within the separation region of the leading ripple, the drag force exerted by the air flow on the trailing ripple diminishes, causing it to slow down and merge with a faster advancing ripple. Larger ripples are formed which protrude further into the air boundary layer and gain higher form drag. Thus, ripple speeds tend to increase indefinitely in the flow direction.

Conclusions

Air-driven liquid films were found to develop interfacial waves except for very low air speeds. Uniform sinusoidal waves were observed over a limited range of air speeds while higher air speeds resulted in the formation of solitary ripples. The ripple regime prevailed over most of the operating conditions of the present study.

Pressure measurements on the contour of solid waves similar in shape to the liquid ripples demonstrate the fact that the motion of liquid films in parallel two-phase flow is dominated by drag forces exerted by air on interfacial disturbances which transport the bulk of the liquid flow rate.

References

1. J. Larras and A. Claria, Houille Blanc 6, 674 (1960).
2. K. Zagustin, E.Y. Hsu, R.L. street and B. Perry, Dept. of Civil Engineering, Stanford University, Technical Report No.60 (1966).
3. D. Zilker, G.W. Cook and T.J. Hanratty, J. Fluid Mech. 82, 29 (1977).
4. D. Zilker and T.J. Hanratty, J. Fluid Mech. 90, 257 (1979).